JOURNAL OF MATERIALS SCIENCE 15 (1980) 2167–2174

Phase relationships in the system Cr-W-O and thermodynamic properties of $CrWO_4$ and Cr_2WO_6

K. T. JACOB
Department of Metallurgy and Materials Science, University of Toronto, Toronto, Canada

The phase diagram of the Cr–W–O system at 1000° C was established by metallographic and X-ray identification of the phases present after equilibration in evacuated silica capsules. Two ternary oxide phases, $CrWO_4$ and Cr_2WO_6 were detected. The oxygen potential over the three-phase mixtures, $W + Cr_2O_3 + CrWO_4$, $WO_{2.90} + CrWO_4 + Cr_2WO_6$ and $Cr_2O_3 + CrWO_4 + Cr_2WO_6$, were measured by solid state cells incorporating Y_2O_3 stabilized ZrO_2 electrolyte and Ni + NiO reference electrode. The Gibbs' energies of formation of the two ternary phases can be represented by the following equations

$$W(s) + \tfrac{1}{2}\,Cr_2O_3(s) + \tfrac{5}{4}\,O_2(g) \rightarrow CrWO_4(s)$$

$$\Delta G^0 = -172\,047 + 48.725T\ (\pm 230)\ \text{cal mol}^{-1}$$

$$Cr_2O_3(s) + WO_3(s) \rightarrow Cr_2WO_6(s)$$

$$\Delta G^0 = -3\,835 + 0.235T\ (\pm 500)\ \text{cal mol}^{-1}$$

1. Introduction

Many tungsten fibre reinforced metal composites have interesting high temperature properties. For an evaluation of their high temperature oxidation resistance ternary and higher order phase diagrams are necessary. Chromium is one of the alloying elements which is usually present in the matrix to enhance its resistance to oxidation. The nature of the interaction of oxygen and chromium with the tungsten fibre is an important aspect of the oxidation characteristics of these composites.

By identifiying the equilibrium phases in the Cr–W–O system at 1000° C by metallography and X-ray diffraction, and using information available in the literature on the binary systems, a ternary phase diagram has been developed in this study. Two ternary compounds, $CrWO_4$ and Cr_2WO_6, have been identified. The compound, $CrWO_4$, has not been reported in the literature. The stability of the Cr_2WO_6 phase between 1000 and 1200° C was recognized by Trunov and Koyba [1]. Its crystal structure was determined by Bayer [2] as an inverse trirutile type, which differs from the normal in the metal stacking sequence. During a recent investigation of the pseudo-binary Cr_2O_3–WO_3 system, Gardinier and Chang [3] have confirmed the existance of Cr_2WO_6 between 900 and 1350° C. Three condensed phases co-exist in eight regions of the Gibbs' triangle representing the Cr–W–O system at 1000° C. The oxygen potential over five of these eight three-phase regions are identical to those that exist in the limiting binary systems, or can be calculated from the binary data. The oxygen potentials over the remaining three-phase regions have been measured by solid oxide galvanic cells. From this information, the standard Gibbs' energies of formation of $CrWO_4$ and Cr_2WO_6 were calculated as a function of temperature. Ternary phase relationships at other temperatures can readily be derived from the thermodynamic data.

This research is part of a wider programme of experimental and computational studies on phase diagrams relevant to the oxidation behaviour of tungsten fibre reinforced composites. The first of this study on the Ni–W–O system was published earlier [4].

0022–2461/80/092167–08$02.80/0

TABLE I The phases in equilibrium in different regions of the Cr–W–O system at 1000° C identified by metallography and X-ray diffraction

Composition of the pellets before equilibration (mol %)					Phases present after equilibration at 1000° C
Cr	W	Cr_2O_3	WO_2	WO_3	
72.22	22.22	—	5.56	–	$\alpha'(Cr) + \alpha''(W) + Cr_2O_3$
78.57	7.14	–	–	14.29	$\alpha' + \alpha'' + Cr_2O_3$
25.00	68.75	6.25	–	–	$\alpha' + \alpha'' + Cr_2O_3$
41.67	33.33	8.33	16.67	–	$\alpha' + \alpha'' + Cr_2O_3$
32.86	52.86	–	–	14.29	$\alpha'' + Cr_2O_3$
83.87	–	12.90	–	3.23	$\alpha' + Cr_2O_3$
25.00	41.67	–	33.33	–	$W + Cr_2O_3 + CrWO_4$
56.01	–	7.99	–	36.00	$W + Cr_2O_3 + CrWO_4$
–	33.33	33.33	–	33.33	$W + Cr_2O_3 + CrWO_4$
11.66	66.13	–	–	22.21	$W + WO_2 + CrWO_4$
–	54.21	12.49	–	33.30	$W + WO_2 + CrWO_4$
–	–	16.67	83.33	–	$W + WO_2 + CrWO_4$
16.67	–	–	16.67	66.67	$WO_2 + WO_{2.72} + CrWO_4$
–	17.56	16.36	–	66.07	$WO_2 + WO_{2.72} + CrWO_4$
14.29	–	–	–	85.71	$WO_{2.72} + WO_{2.90} + CrWO_4$
–	6.68	20.00	–	73.32	$WO_{2.90} + CrWO_4 + Cr_2WO_6$
–	7.47	30.62	–	61.90	$WO_{2.90} + CrWO_4 + Cr_2WO_6$
7.16	–	50.00	–	42.84	$CrWO_4 + Cr_2WO_6 + Cr_2O_3$
8.33	–	41.67	–	50.00	$CrWO_4 + Cr_2WO_6 + Cr_2O_3$

α' is a Cr-rich solid solution containing 7 at% W.
α'' is a W-rich solid solution containing 10.3 at% Cr.

2. Experimental methods

2.1. Materials

Fine powders of analar grade tungsten and tungsten oxides (WO_3) were obtained from the Fisher Chemical Co., while chromium (99.9%) and chromium oxide (Cr_2O_3, 99.8%) powders were supplied by the Alfa Division of Ventron Corporation. The tungsten trioxide was further dehydrated by heating at 400° C in an alumina boat in dry oxygen. The suboxides of tungsten (WO_2, $WO_{2.72}$ and $WO_{2.9}$) were prepared by reacting mixtures of $W + WO_3$ in the required ratios in evacuated silica capsules at 1000° C for 24h. The ternary compounds $CrWO_4$ and Cr_2WO_6 were prepared from W, WO_3 and Cr_2O_3 by prolonged heating at 1000° C. The argon gas, which was used as the atmosphere during the emf measurements, was 99.998% pure and was further dried and deoxidized by passing through copper turnings at 450° C and titanium granules at 800° C. Fully stabilized Y_2O_3–ZrO_2 solid electrolyte tubes were obtained from the Zircoa Corporation.

2.2. Apparatus and procedure

2.2.1. Phase relations.

Fine powders of metals and oxides in preselected proportions were mixed in a ball mill and compressed into pellets of 5 mm diameter and 2.5 mm thickness by a hydraulic press at a pressure of 2500 kg m^{-2}. The compositions of the starting pellets are given in Table I. The pellets, wrapped in coarse platinum gauze, were placed in closed end silica tubes, which were evacuated to a pressure of 10^{-4} atm and sealed under vacuum. The silica capsules were placed in a muffle furnace maintained at 1000° C. The temperature was held to within ± 3° C by a solid state controller. The temperature variation between the various silica capsules in the muffle furnace was less than ± 4° C. The average temperature was monitered by a Pt/Pt–13% Rh thermocouple. Preliminary experiments indicated that approximately 2 to 5 days were required to attain equilibrium. To ensure that the pellets were fully equilibrated, actual equilibration times up to 7 days were employed. At the end of the equilibration period the capsules were quenched in liquid nitrogen. The pellets were mounted and the phases present were identified by metallographic and X-ray diffraction analysis. Conventional preparatory techniques were used in the analysis.

2.2.2. EMF measurements

From a study of the phases present after equilibration, eight regions were identified on the Gibbs' ternary triangle for the Cr–W–O system where three condensed phases co-exist. The oxygen potentials corresponding to a number of these regions were measured by the following solid state electrochemical cells, based on Y_2O_3 stabilized ZrO_2 as the electrolyte and using Ni + NiO as the reference electrode

$$\text{Pt, Ni + NiO/Y}_2\text{O}_3 - \text{ZrO}_2\text{/WO}_2 + \text{WO}_{2.72}\text{, Pt} \qquad \text{I}$$

$$\text{Pt, Ni + NiO/Y}_2\text{O}_3 - \text{ZrO}_2\text{/W + WO}_2 + \text{CrWO}_4\text{, Pt} \qquad \text{II}$$

$$\text{Pt, Ni + NiO/Y}_2\text{O}_3 - \text{ZrO}_2\text{/W + CrWO}_4 + \text{Cr}_2\text{O}_3\text{, Pt} \qquad \text{III}$$

$$\text{Pt, Ni + NiO/Y}_2\text{O}_3 - \text{ZrO}_2\text{/CrWO}_4 + \text{Cr}_2\text{WO}_6 + \text{Cr}_2\text{O}_3\text{, Pt} \qquad \text{IV}$$

$$\text{Pt, Ni + NiO/Y}_2\text{O}_3 - \text{ZrO}_2\text{/WO}_{2.90} + \text{CrWO}_4 + \text{Cr}_2\text{WO}_6\text{, Pt} \qquad \text{V}$$

The measurements on cells I and II were performed to check the apparatus. The emfs of these two cells can be calculated from the thermodynamic data on WO_2 and $WO_{2.72}$ phases available in the literature.

The reference and working electrodes were prepared in the form of pellets by double end compression of an intimate equimolar mixture of component phases and subsequent sintering in evacuated quartz capsules. Examination of the pellets by optical microscopy and X-ray diffraction showed that there was no significant change in their composition during the sintering operation. The pellets were polished and spring loaded against either side of a flat-ended Y_2O_3–ZrO_2 tube. The geometry of the arrangement is shown in Fig. 1. A static inert blanket was maintained over the working electrode, while a stream of argon gas (100 ml min^{-1}) was maintained over the Ni + NiO reference electrode. The emfs of the cells were monitored as a function of temperature in the range 750 to 1025° C by a "Keithley" digital voltmeter. The reversibility of the emf was checked by passing small currents through the cell in either direction. In each case the emf was found to return to the steady state value before the coulometric titration. The emf was independent of the flow rate of inert gas in the range 50 to 250 ml min^{-1}, and was reproducible after prolonged temperature changes. The time required to attain steady ems varied from 6 to 15 h depending on the composition of the electrode and temperature. No significant change in the composition of the electrodes was detected by X-ray diffraction analysis after emf measurements.

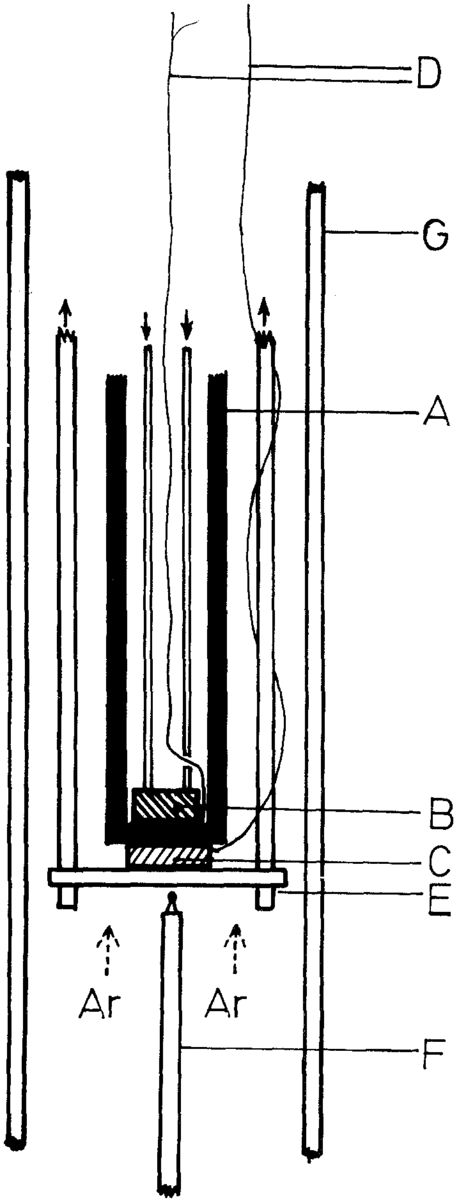

Figure 1 Schematic diagram of the cell used in emf measurements. A–solid electrolyte tube, B–working electrodes C–reference electrode (Ni + NiO), D–Pt leads E–an arrangement of alumina rods and slabs for spring loading the reference electrode against the solid electrolyte, F–Pt/Pt–13% Rh Thermocouple, G–alumina tube.

3. Results, analysis and discussion

3.1. Phase diagram

The phases identified after equilibration of various condensed phase mixtures are summarized in Table I. At 1000° C there is a miscibility gap in

TABLE II The X-ray diffraction pattern for $CrWO_4$

Number	Intensity	d_{hkl}
1	100	2.47
2	89	3.33
3	75	4.63
4	65	3.22
5	51	1.70
6	40	1.68
7	40	2.20
8	30	2.32
9	23	2.05
10	20	1.67
11	19	1.36
12	18	2.92
13	15	1.60
14	14	1.44
15	14	1.81
16	13	1.33
17	11	1.45
18	11	1.48
19	8	1.54
20	7	1.38

the binary Cr–W system. From the lattice parameters of the equilibrium phases the Cr-rich solid solution phase (α') was found to contain 7 at% W, while the W-rich phase had 10.3 at% Cr. These values are in reasonable agreement with earlier studies by Trzenbiatowski *et al.* [5], Greenaway [6], Den Broeder [7], and Margaria *et al.* [8].

Two ternary oxide phases were identified in this study. The compound $CrWO_4$ has not been reported in the literature, while a diffraction pattern for Cr_2WO_6 obtained in this study agreed with that given by Bayer [2]. The X-ray diffraction pattern for the new compound, $CrWO_4$, is shown in Table II. Most of the lines can be identified with an orthorhombic unit cell with lattice constants $a = 9.99$ Å, $b = 10.18$ Å and $c = 18.23$Å. The diffraction patterns for this compound in different phase regions were identical, suggesting a narrow range of nonstoichiometry. The valencies of 5 or 2 for Cr in $CrWO_4$ are interesting, especially since there are not stable oxides with corresponding valencies in the binary Cr–O system at high temperatures.

A ternary phase diagram of the Cr–W–O system at 1000° C composed from the present results is shown in Fig. 2. This ternary diagram is consistant with well known binary diagrams of W–O and Cr–O systems. Application of the phase

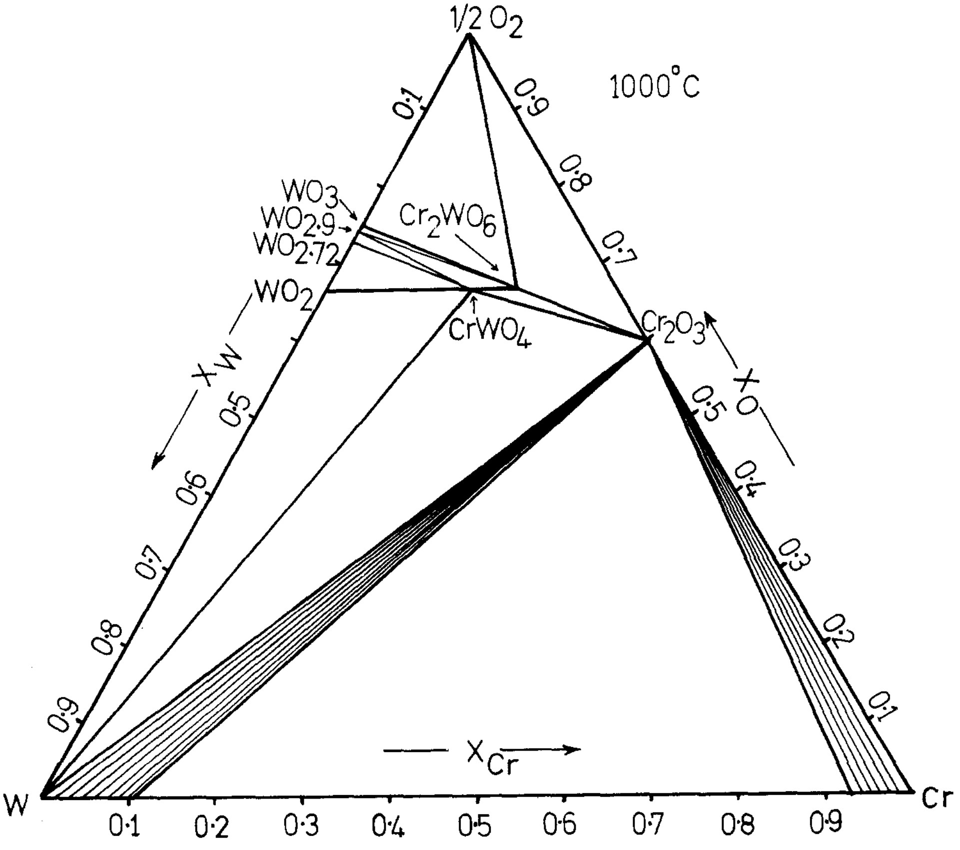

Figure 2 Gibbs triangle representation of phase relations in the Cr–W–O system at 1000° C.

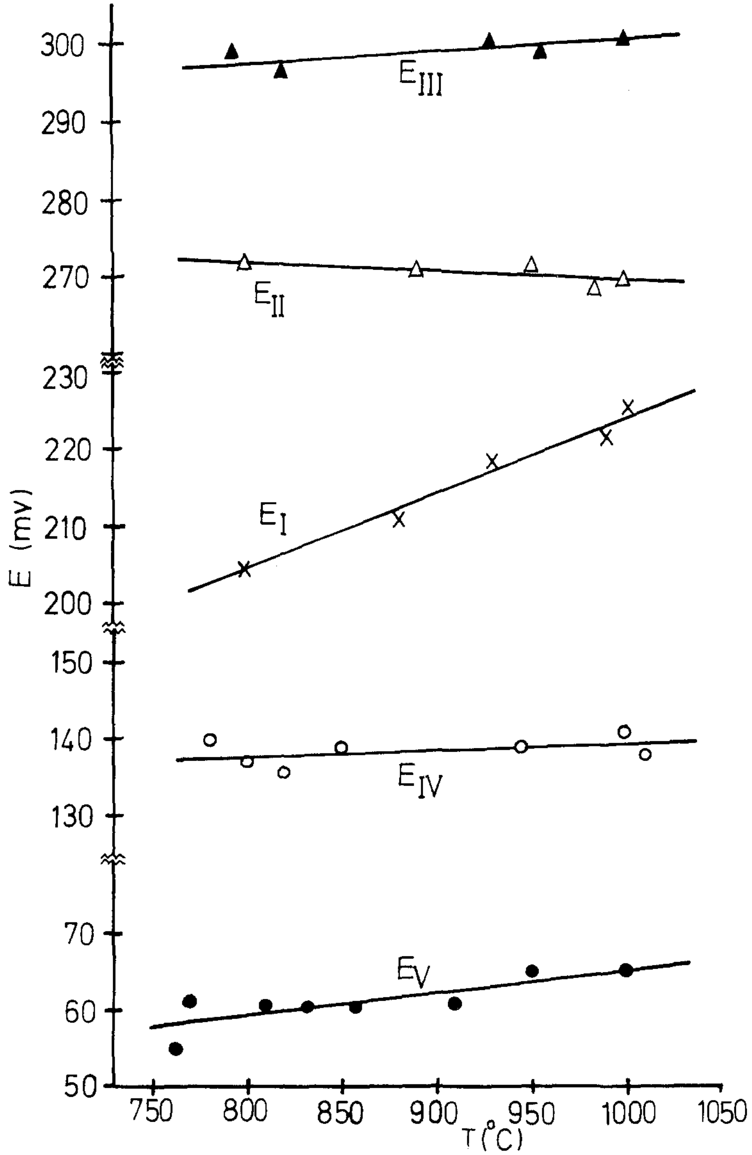

Figure 3 The variation of the emf of cells I to V with temperature.

rule indicates that the oxygen potential must be constant in those regions where three condensed phases co-exist at any fixed temperature. Across the two phase regions the oxygen potential would vary with composition.

3.2. Oxygen potentials and Gibbs' energies

The emfs of cells I to V are plotted in Fig. 3 as a function of temperature. The emfs can be represented by the following linear equations

$$E_I = 98.3 + 9.9 \times 10^{-2}\, T\,(\pm 1.5)\,\text{mV} \quad (1)$$

$$E_{II} = 283 + 1.04 \times 10^{-2}\, T\,(\pm 1)\,\text{mV} \quad (2)$$

$$E_{III} = 279 + 1.73 \times 10^{-2}\, T\,(\pm 2)\,\text{mV} \quad (3)$$

$$E_{IV} = 128 + 8.5 \times 10^{-2}\, T\,(\pm 2.5)\,\text{mV} \quad (4)$$

$$E_V = 26.3 + 3.06 \times 10^{-2}\, T\,(\pm 2)\,\text{mV}. \quad (5)$$

The emf of these solid state cells with an oxygen ion conducting electrolyte is related to the difference in the chemical potentials of oxygen at the two electrodes.

$$nFE = \Delta\mu'_{O_2} - \Delta\mu''_{O_2} = RT \ln (P'_{O_2}/P''_{O_2}) \quad (6)$$

where n is the number of electrons involved in the electrode reaction and has a value of 4, F is the Faraday constant and E is the emf. The oxygen potential of the Ni + NiO reference is well established and may be represented by the equation [9]

TABLE III Comparison of oxygen potentials of the mixtures W + WO_2 and WO_2 + $WO_{2.72}$

Source	$\Delta\mu_{O_2}'$ (kcal mol^{-1})					
	800° C		900° C		1000° C	
	W + WO_2	WO_2 + $WO_{2.72}$	W + WO_2	WO_2 + $WO_{2.72}$	W + WO_2	WO_2 + $WO_{2.72}$
Rizzo *et al.* [10]	−93.73	−87.07	−89.67	−84.07	−85.61	−81.06
Janaf Tables [11]	−94.36	−88.54	−90.26	−85.14	−86.19	−81.76
This study	−93.50	−87.25	−89.32	−84.11	−85.17	−80.96

$$\Delta\mu_{O_2}(\mathrm{Ni + NiO}) = -111\,930 + 40.58\,T \text{ cal mol}^{-1}. \quad (7)$$

The oxygen potentials of the working electrodes calculated from Equations 6 and 7 are given below, along with the chemical equations that define the oxygen potentials. For the reaction,

$$2.78\,WO_2 + O_2 \rightarrow 2.78\,WO_{2.72}$$

$$\Delta G^0 = \Delta\mu_{O_2} = -121\,000 + 31.45\,T\,(\pm 150) \text{ cal mol}^{-1} \quad (8)$$

$$W + O_2 \rightarrow WO_2$$

$$\Delta G^0 = \Delta\mu_{O_2} = -138\,050 + 41.54\,T\,(\pm 100) \text{ cal mol}^{-1} \quad (9)$$

$$\tfrac{4}{5}\,W + \tfrac{2}{5}\,Cr_2O_3 + O_2 \rightarrow \tfrac{4}{5}\,WCrO_4$$

$$\Delta G^0 = \Delta\mu_{O_2} = -137\,640 + 38.98\,T\,(\pm 200) \text{ cal mol}^{-1} \quad (10)$$

$$4CrWO_4 + 2Cr_2O_3 + O_2 \rightarrow 4Cr_2WO_6$$

$$\Delta G^0 = \Delta\mu_{O_2} = -123\,760 + 39.8\,T\,(\pm 250) \text{ cal mol}^{-1} \quad (11)$$

$$4.44\,CrWO_4 + O_2 \rightarrow 2.22\,Cr_2WO_6 + 2.22\,WO_{2.90}$$

$$\Delta G^0 = \Delta\mu_{O_2} = -114\,360 + 37.76\,T\,(\pm 200) \text{ cal mol}^{-1}. \quad (12)$$

Since the X-ray diffraction patterns of the various condensed phases in the pellets after emf measurements were almost identical to their individual patterns in the pure state, mutual solubility is negligible, and their activities are equal to unity. The standard free energy changes for the above reactions are therefore equal to the corresponding chemical potentials of oxygen. The error limits correspond to twice the standard deviation in the emf measurements. The working electrode in cell II contains a mixture of W + WO_2 + $CrWO_4$. The oxygen potential over this three phase mixture would be the same as that over the W + WO_2 mixture and is related to the free energy of formation of WO_2 given by Equation 9.

The oxygen potentials of W + WO_2 and WO_2 + $WO_{2.72}$ mixtures measured in this study are compared in Table III with those reported by Rizzo *et al.* [10], and the tabulated values in Janaf tables [11]. The good agreement with the earlier electrochemical measurements by Rizzo *et al.* suggest that the present emf studies are free from any significant systematic errors. The Janaf values, based primarily on calorimetric data, are approximately 1 kcal more negative. In the light of the new emf measurements, the Janaf values may require minor revision.

The Gibbs' free energy of formation of the new compound, $CrWO_4$, from Cr_2O_3, W and O_2(g) is given by Equation 10. The free energy of formation of Cr_2WO_6 can be derived from either Equation 11 or 12, using results obtained in the study for $CrWO_4$ and the data of Rizzo *et al.* [10] for $WO_{2.90}$. For the reaction,

$$W + Cr_2O_3 + \tfrac{3}{2}\,O_2 \rightarrow Cr_2WO_6$$

the standard free energy change calculated from Equation 11 based on measurements in cell IV, is

$$\Delta G^0 = -202\,990 + 58.68\,T\,(\pm 300) \text{ cal mol}^{-1} \quad (13)$$

while the value obtained from Equation 12 which is based on the emf of cell V is

$$\Delta G^0 = -203\,090 + 58.68\,T\,(\pm 600) \text{ cal mol}^{-1} \quad (14)$$

At a temperature of 1000° C, the values given by Equations 13 and 14 agree to within ± 100 cal. The good internal consistancy between measurements on cells IV and V is encouraging. Using the data of Rizzo *et al.* [10] for WO_3, the free energy of formation of Cr_2WO_6 from component oxides can be expressed as

$$Cr_2O_3 + WO_3 \rightarrow Cr_2WO_6$$

$$\Delta G^0 = -3\,835 + 0.235\,T\,(\pm 500) \text{ cal mol}^{-1} \quad (15)$$

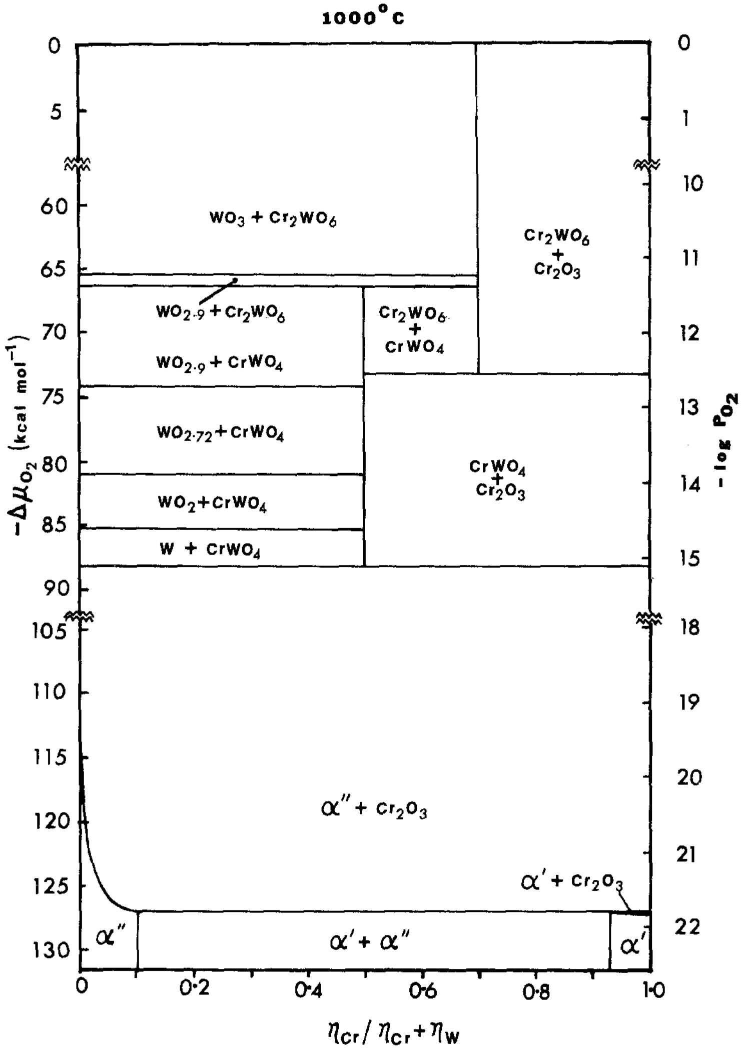

Figure 4 Oxygen potential–composition diagram for the Cr–W–O system at 1000° C.

3.3. Oxygen potential diagram for the Cr–W–O system

The oxygen potential diagram at 1000° C, constructed from the results of this study and additional thermodynamic data available in the literature on binary phases in the W–O [10] and Cr–O [12] systems, is shown in Fig. 4. This type of diagram is more useful in the interpretation of the corrosion behaviour in gas mixtures than the Gibbs' ternary representation. Corrosion products at any oxygen partial pressure and alloy composition can be readily identified. The only disadvantage is that the oxygen nonstoichiometry of phases cannot be depicted. The various three-phase equilibria are shown as horizontal lines in this plot. The oxygen potential variations in the two-phase regions, $\alpha' + Cr_2O_3$ and $\alpha'' + Cr_2O_3$, are calculated from estimated activities in the binary Cr–W system and thermodynamic data on Cr_2O_3 [12].

$$\tfrac{4}{3}\,Cr + O_2 \rightarrow \tfrac{2}{3}\,Cr_2O_3$$

$$\Delta G^0 = -177\,810 + 39.89\,T\,(\pm\,150)\ \text{cal mol}^{-1} \qquad (16)$$

$$\Delta\mu_{O_2} = \Delta G^0 - \tfrac{4}{3}\,\Delta\mu_{Cr} \qquad (17)$$

The activities in the Cr–W binary systems are estimated from the solid solubility limits obtained in this study using the sub-regular solution model [13]. The activity of Cr and the excess free energy of mixing are given by the expressions

$$\Delta\mu_{Cr} = RT\ln a_{Cr} = RT\ln X_{Cr} + 8465\,X_W^2 - 1790\,X_W^3 \qquad (18)$$

$$\Delta G^{M,Ex} = X_{Cr}X_W\,(7600\,X_{Cr} + 6735\,X_W) \qquad (19)$$

where *a* and *X* are the activities and mole fractions respectively. Fig. 4 shows that the new compound, $CrWO_4$ is stable only over a limited range of oxygen partial pressure, $-11.382 > \log p_{O_2} > -15.11$, at 1000° C.

Acknowledgement

The author is grateful to the Natural Sciences and Engineering Research Council Canada for partial support of this research.

References

1. V. K. TRUNOV and L. M. KOVBA, *Izv. Akad. Nauk SSSR, Neorg. Mater.* **2** (1966) 151.
2. G. BAYER, *J. Amer. Ceram. Soc.* **43** (1960) 495.
3. C. F. GARDINIER and L. L. Y. CHANG, *J. Amer. Ceram. Soc.* **61** (1978) 376.
4. K. T. JACOB, *J. Mater. Sci.* **12** (1977) 1647.
5. W. TRZEBIATOWSKI, H. PLOSZEK and J. LOBZOWSKI, *J. Anal. Chem.* **19** (1947) 93.
6. H. T. J. GREENAWAY, *J. Inst. Metals* **80** (1951) 589.
7. F. J. A. DEN BROEDER, *Acta Metall.* **20** (1972) 319.
8. T. MARGARIA, C. ALLIBERT, I. ANSARA and J. DRIOLE, *High Temperatures-High Pressures* **8** (1976) 451.
9. B. C. H. STEELE in "Electromotive force measurements in high temperature systems", edited by C. B. Alcock, (Inst. Min. Met., London, 1968) p. 3.
10. F. E. RIZZO, L. R. BIDWELL and D. F. FRANK, *Trans. Met. Soc. AIME* **239** (1967) 1901.
11. D. R. STULL and H. PROPHET, *JANAF Thermochemical Tables, NSRDS – NBS 37* (U.S. Department of Commerce, Washington, D. C. 1971).
12. K. T. JACOB, *J. Electrochem. Soc.* **124** (1977) 1827.
13. H. K. HARDY, *Acta Metall.* **1** (1953) 202.

Received 27 November 1979 and accepted 15 April 1980.